Journal of Alloys and Compounds 514 (2012) 205–209

Contents lists available at SciVerse ScienceDirect

Journal of Alloys and Compounds

journal homepage: www.elsevier.com/locate/jallcom

Fabrication and properties of $Bi_{2-x}Ag_{3x}S_3$ thermoelectric polycrystals

Zhen-Hua Ge, Bo-Ping Zhang*, Yi-Qiang Yu, Peng-Peng Shang

School of Materials Science and Engineering, University of Science and Technology Beijing, Xueyuan Road 30, Beijing 100083, China

ARTICLE INFO

Article history:
Received 6 September 2011
Received in revised form
14 November 2011
Accepted 14 November 2011
Available online 22 November 2011

Keywords:
Bi_2S_3
Ag doping
Thermoelectric
$AgBi_3S_5$

ABSTRACT

$Bi_{2-x}Ag_{3x}S_3$ ($x = 0$–0.06) polycrystals were fabricated by mechanical alloying (MA) and spark plasma sintering (SPS). The phase, microstructure, electrical and thermal transport properties were investigated with a special emphasis on the influence of Ag doping content. All the $Bi_{2-x}Ag_{3x}S_3$ powders can be indexed as single phase with an orthorhombic symmetry, a second $AgBi_3S_5$ phase in SPSed bulks occurs as the doping contents $x \geq 0.02$, which enhances the electrical conductivity, resulting in improvement of electrical transport properties for $Bi_{2-x}Ag_{3x}S_3$ bulk samples. A maximum ZT value reached 0.23 at 573 K for the $Bi_{1.99}Ag_{0.03}S_3$ sample, which is 130% higher than that (0.11) of the pure Bi_2S_3.

1. Introduction

Thermoelectric (TE) energy conversion has received more and more interest because of its promising application in directly converting both the existing heat in nature and waste heat generated in industry [1,2]. High performance TE materials should possess large Seebeck coefficient, high electrical conductivity and low thermal conductivity. The efficiency of energy conversion for TE materials is mainly determined by the dimensionless TE figure of merit ZT, which is defined as $ZT = \alpha^2\sigma T/\kappa$, where T, α, σ and κ, are the absolute temperature, Seebeck coefficient, electrical conductivity, and thermal conductivity, respectively [3].

The compounds A_2B_3 (where A = Bi, Sb and B = S, Se, Te) are considered to be most promising for TE applications [4]. Bi–Te-based [5,6] and Pb–Te-based [7,8] compounds show the best TE properties near room temperature and near 800 K, respectively. However, the common feature of these materials is that they contain significant amount of Te, which is a scarce element in the crust of the earth. Hence the Te price is likely to rise sharply if Te-based thermoelectric materials reach mass markets. A broad search for more inexpensive alternatives is therefore warranted. Bismuth sulfide (Bi_2S_3) also belongs to A_2B_3 family compounds [9] and is a layered semiconductor with a direct band gap 1.3 eV, which results in a high electrical resistivity, therefore, a little attention has been paid to Bi_2S_3 in TE development, and it was subsequently neglected in favor of Bi–Te-based compounds [5,6]. Hopefully, the Bi_2S_3 compound will be a robust alternative TE material for applications if the electrical resistivity could be reduced [10–12].

Chen et al. [10] first reported the TE properties below room temperature of Bi_2S_3, which was proposed as a good TE material for its high Seebeck coefficient (about 400 μV/K) and low thermal conductivity (<1 $W\,m^{-1}\,K^{-1}$), but a marginal figure of merit ($ZT = 0.055$) because of high electrical resistivity (0.05 Ωm). Shaban et al. [11] reported that the anisotropic electrical transport properties for single crystal Bi_2S_3. Zhao and his coworkers [12] recently found sulfur-deficient and texturing processing can effectively lower electrical resistivity, resulting in an improvement in power factor. A ZT value of 0.11 at 523 K was obtained by combination of enhanced power factor and natural low thermal conductivity. Though Ag is expense and not abundant, but which usually were used as a dopant in smaller quantities. Kyratsi et al. [13] found the uneven distribution of the atoms and electronic replacement phenomenon of the atoms in the lattice for the quaternary alloys K–Bi–Sb–Se and Ag–Pb–Sb–Te. The complexity of these structures is beneficial to improve the TE performance. Cui et al. [14] revealed that doping Ag into Bi–Te base alloy reduces thermal conductivities and contributes to the high ZT value, in which an Ag-doped $(Bi_2Te_3)_{0.9}$–$(Bi_{1.6}Ag_{0.4}Se_3)_{0.1}$ alloy showed 30% TE improvement compared with Ag-free alloys. These results motivated us to expand our investigations of Bi_2S_3 and for this system pursue many of the new concepts and ideas developed for Bi–Te based and Pb–Te based compounds, which have been so successful in producing record breaking performance. Compared with conventional melting or grinding techniques, mechanical alloying (MA) has several advantages such as avoiding segregation from melting state, preparing nanometer powder in short time. MA has been recently applied

* Corresponding author. Tel.: +86 10 62334195.
E-mail address: bpzhang@ustb.edu.cn (B.-P. Zhang).

0925-8388/$ – see front matter © 2011 Elsevier B.V. All rights reserved.
doi:10.1016/j.jallcom.2011.11.072

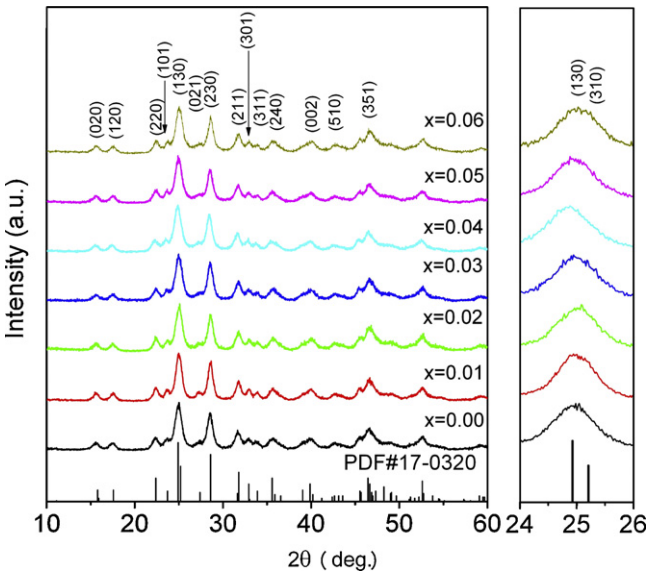

Fig. 1. XRD patterns of the MA-treated $Bi_{2-x}Ag_{3x}S_3$ ($x = 0, 0.01, 0.02, 0.03, 0.04, 0.05, 0.06$) powders.

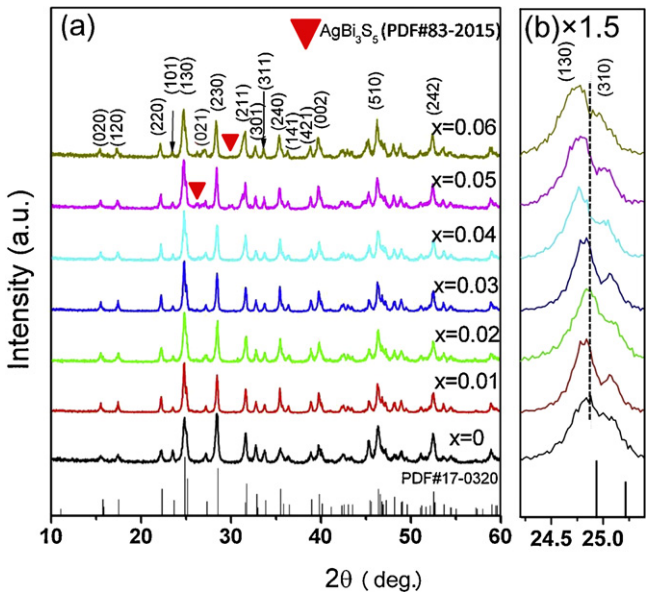

Fig. 2. XRD patterns of the $Bi_{2-x}Ag_{3x}S_3$ ($x = 0, 0.01, 0.02, 0.03, 0.04, 0.05, 0.06$) bulks sintered by applying SPS at 673 K.

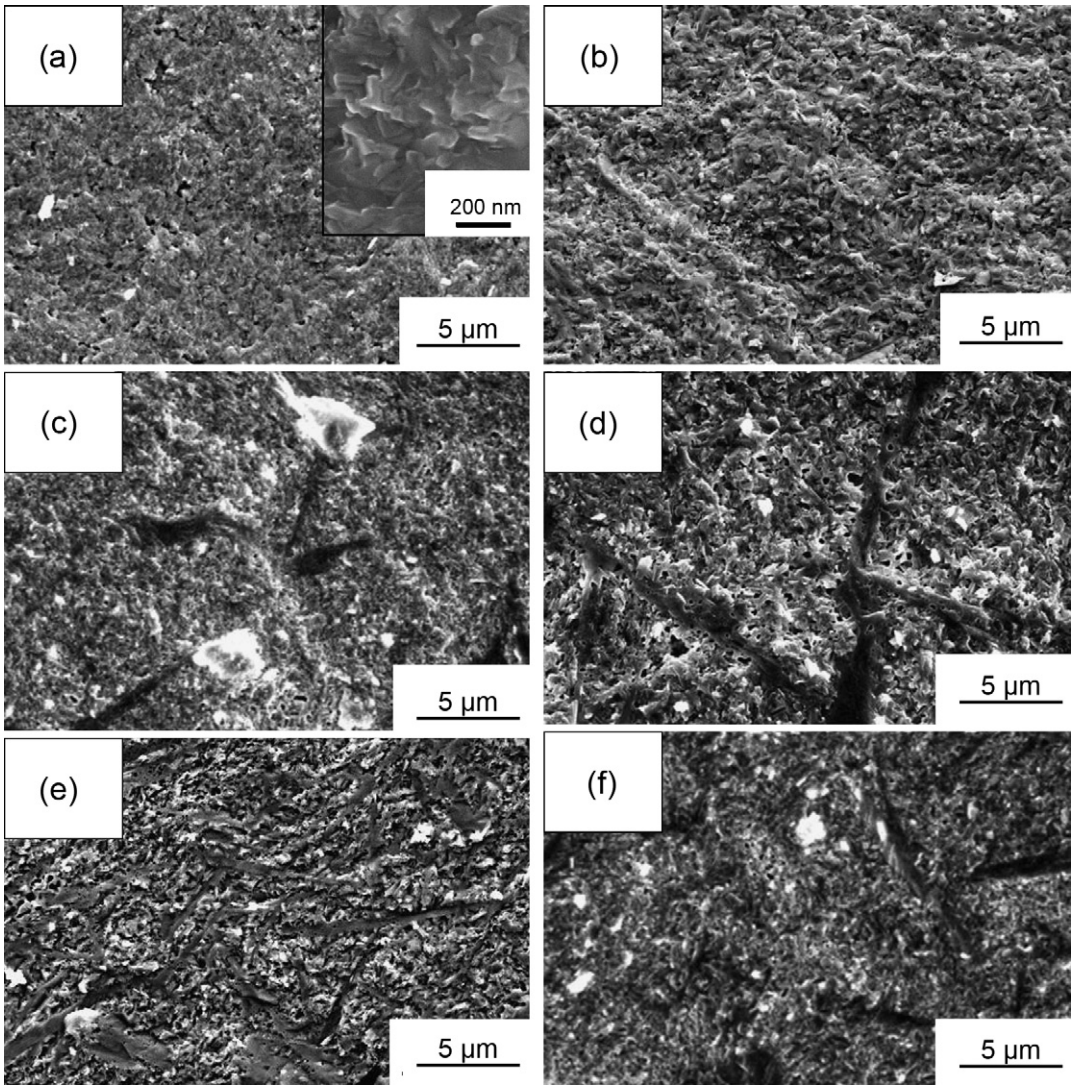

Fig. 3. Field emission scanning electron microscopy of the fractured surfaces for the $Bi_{2-x}Ag_{3x}S_3$ bulks. (a) $x = 0$, (b) $x = 0.01$, (c) $x = 0.02$, (d) $x = 0.04$, (e) $x = 0.05$ and (f) $x = 0.06$.

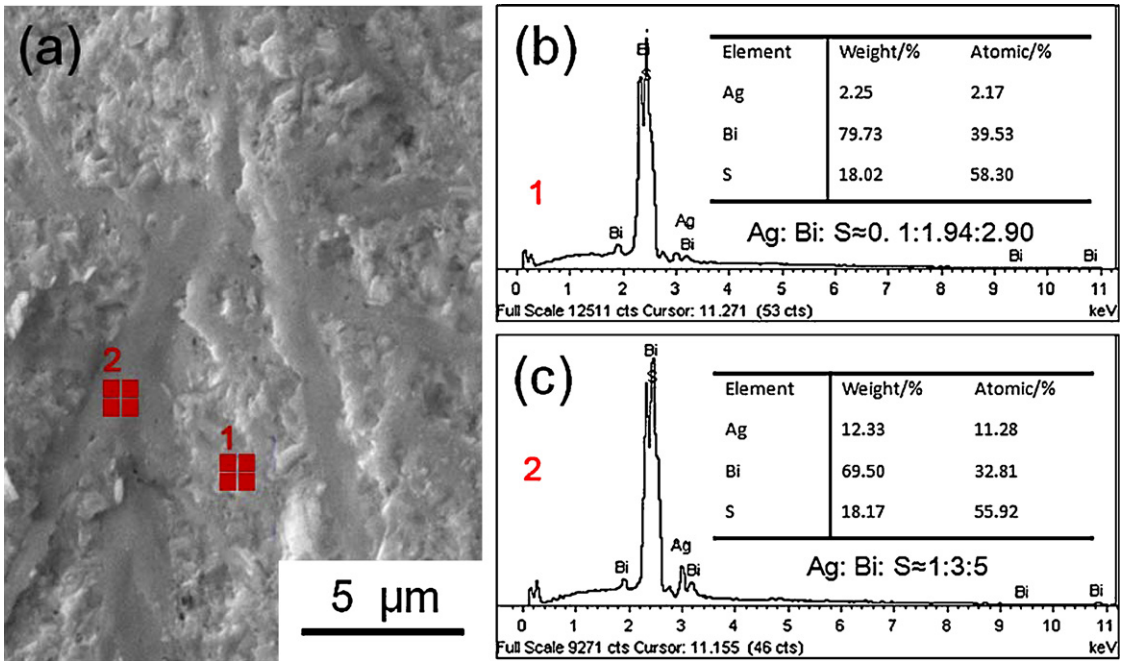

Fig. 4. FESEM micrograph (a) and EDS spectra (b and c) taken from the matrix (position 1) and the strip-like structure (position 2) for the $Bi_{1.94}Ag_{0.18}S_3$ ($x = 0.06$) bulk sample.

to fabricate nano-sized alloys [15], and MA shows an outstanding advantage on the fabrication for the compounds composed of low melting point or volatile elements. Spark plasma sintering (SPS) is suitable for fabricating fine-grained materials, because SPS can restrict grain growth by reducing sintering temperature and sintering time [16]. In this work, Ag-doped ternary $Bi_{2-x}Ag_{3x}S_3$ ($x = 0$–0.06) alloys were fabricated by MA and SPS techniques, and the effect of Ag content on their thermoelectric properties was investigated.

2. Experimental

Commercial high-purity powders of 99.99% Bi, 99.9% Ag and 99.9% S under the same 200 mesh were used as raw materials. The powders with a chemical composition of $Bi_{2-x}Ag_{3x}S_3$ ($x = 0$–0.06) were ball-milled at 400 rpm for 15 h in a mixture atmosphere of high-purity argon (95%) and hydrogen (5%) gases using a planetary ball mill (QM-1SP2, Nanjing University, China). Then the as-synthesized powders were milled at 300 rpm for 1 h in an absolute ethyl alcohol atmosphere. Stainless steel vessels and balls were used, and the weight ratio of the ball to powder was kept at 20:1. The ball-milled powders were sintered at 673 K for 5 min in a Ø20 mm graphite moulds under a axial pressure of 40 MPa in a vacuum using the SPS system (Sumitomo SPS1050, Japan). Phase structure was analyzed by X-ray diffraction (XRD, CuKα, BrukerD8, Germany). The morphologies of fractographs and energy dispersive spectrum (EDS) of bulks were investigated by a field emission scanning electron microscopy (FESEM, SUPRATM 55, Germany). The TE properties were evaluated along the sample section perpendicular to the pressing direction of SPS. The Seebeck coefficient and electrical resistivity were measured at 323–573 K in a helium atmosphere using a Seebeck coefficient/electric resistance measuring system (ZEM-2, Ulvac-Riko, Japan). The thermal conductivity κ was calculated by the relationship of $\kappa = DC_p d$ with a specific heat C_p, whose value is about 0.21–0.24 from room temperature to 573 K, measured by using a thermal analyzing apparatus (Dupont 1090B, USA), density measured by the Archimedes method and the thermal diffusivity D measured by a laser flash method (NETZSCH Laser Flash Apparatus LFA427, Germany).

3. Results and discussion

Fig. 1 shows the XRD patterns of the $Bi_{2-x}Ag_{3x}S_3$ powders ($x = 0$–0.06). The diffraction lines cited from the database of the binary Bi_2S_3 (PDF#17-0320) were also plotted with vertical lines in Fig. 1 for comparison. All the powders show a well-matched pattern to the binary Bi_2S_3 (PDF#17-0320) without any detectable second phase(s), suggesting that Ag enters the lattice of Bi_2S_3 to form a single Bi_2S_3 phase with orthorhombic symmetry during the MA process

Fig. 2 shows the XRD patterns of the $Bi_{2-x}Ag_{3x}S_3$ bulk ($x = 0$–0.06) sintered by applying SPS at 673 K for 5 min. The diffraction peaks of the bulk samples become narrower and sharper than those of the powder samples (Fig. 1) which are attributed to the enhanced crystallinity after SPS. The main phase of all bulk samples show peaks characteristic of orthorhombic Bi_2S_3 (PDF#17-0320). However, some impurity phase of $AgBi_3S_5$ (PDF#83-2015) can be indexed as the doping content exceeds 0.02 mol%. Kim et al. [17] reported that $AgBi_3S_5$ synthesized by flame melting the sealed silica tube filled with Bi, Ag and S powders showed a good conductivity (about 400 S cm^{-1} at 573 K), which is about one order of magnitude higher than that of Bi_2S_3 (about 40 S cm^{-1} at 573 K) [18]. The high conductivity of the second $AgBi_3S_5$ phase plays an important role to decrease electrical resistivity of Bi_2S_3 bulk, which will be discussed later. The (1 3 0) and (3 1 0) diffraction peaks in Fig. 2(b) become distinguishable due to the grain growth, which were overlapped for the powder samples in Fig. 1(b).

For the Ag-free Bi_2S_3 bulk sample, the 2-theta angle of (1 3 0) is 24.90° which is a little lower than 24.93° in the standard card, indicating the enlarged lattice constants due to S volatilization [18,19]. When Ag was added, the shift to lower 2-theta angles for the sample with $x = 0.01$ is attributed to Ag entering into Bi_2S_3 lattice interstices. Further increasing Ag content produces a greater shift of the (1 3 0) diffraction peak to lower angles. This is considered to be from the two existed forms of Ag in the Bi_2S_3 matrix, in which one form is to enter into the host lattice, and the other is to form the second phase $AgBi_3S_5$, as described in the following Eq. (1):

$$Ag_{3x}Bi_{2-x}S_3 \rightarrow yAgBi_3S_5 + Ag_{3x-y}Bi_{2-x-3y}S_{3-5y} \quad (1)$$

Since the second phase is S-rich, an increase of the $AgBi_3S_5$ phase will reduce the S content in Bi_2S_3 matrix and form S vacancies. This will cause a shift in the lattice constant and a shift to lower angles.

Fig. 3 shows the FESEM micrographs of fractured surfaces of $Bi_{2-x}Ag_{3x}S_3$ samples that were formed by SPS at 673 K. It is observed that $Bi_{2-x}Ag_{3x}S_3$ bulks with high relative density (≥92%) have fine grains (100–500 nm) as typically shown in the inset of Fig. 3(a). A strip-like second phase appears after $x \geq 0.02$ and increase with

increasing Ag content. This result is also in good agreement with the XRD analysis. As the x value changes from 0 to 0.01 and 0.02, the relative density of the $Bi_{2-x}Ag_{3x}S_3$ sample increases from 95.8% to 96.5% and 97.1%, respectively. The reason is the activation role of Ag entering the Bi_2S_3 lattice. However, the relative density reduces to 92.1% when x continuously increases to 0.06. The slightly decreased density may be due to the lower density (6.72 g cm^{-3}) of the second $AgBi_3S_5$ phase compared with that (6.81 g cm^{-3}) of the Bi_2S_3 matrix.

Fig. 4 shows FESEM micrograph (a) and EDS spectra (b and c) selected from the matrix (position 1) and a strip-like phase (position 2) for the $Bi_{1.94}Ag_{0.18}S_3$ ($x = 0.06$) bulk sample. Three elements, Ag, Bi, and S, can be found in both the matrix and the strip phase, but the compositions of the two phases are different. As shown in the inset of Fig. 4(b), the atomic ratio of Ag, Bi and S in the matrix (position 1) is about 0.1:1.94:2.90, showing Ag and S contents lower than the nominal ratio of 0.18:1.94:3 ($Bi_{1.94}Ag_{0.18}S_3$ ($x = 0.06$)). The inset of Fig. 4(d) shows the atomic ratio of Ag, Bi, and S for the strip-like phase (position 2) is about 1:3:5, indicating the strip-like structure is $AgBi_3S_5$, which is also in good agreement with the XRD analysis in Fig. 2.

Fig. 5 shows the temperature dependent electrical transport properties for $Bi_{2-x}Ag_{3x}S_3$ ($x = 0$, 0.01, 0.02, 0.04, 0.05, 0.06) bulk samples. As shown in the inset of Fig. 5(a), the electrical resistivity of pure Bi_2S_3 is 1.1×10^{-2} Ωm at room temperature and quickly decreases with increasing temperature, showing typical semiconductor behavior. The electrical resistivity of $Bi_{2-x}Ag_{3x}S_3$ ($x = 0.01$, 0.02, 0.04) shows the same reducing trend with increasing temperature, however, the electrical resistivity of samples ($x = 0.05$ and 0.06) decreases with increasing measurement temperature, peaks at 423 K, and then slightly rises with increasing temperature due to the increased second $AgBi_3S_5$ phase which shows a metal conducting behavior [17]. The electrical resistivity of all the Ag doped Bi_2S_3 alloys are lower than the pure Bi_2S_3 (the inset of Fig. 5(a)). With $x = 0.01$, Ag enters into Bi_2S_3 lattice interstice and results in the increase of electron carrier concentration and in the decrease of resistivity. The defect equation could be given as follows:

$$2Ag \xrightarrow{2Bi_2S_3} 2Ag_i \cdot + 3S_S + 2Bi_{Bi} + 2e' \quad (2)$$

The electrical resistivity (8.7×10^{-4} Ωm) of $Bi_{1.99}Ag_{0.03}S_3$ is about two orders lower than that (1.1×10^{-2} Ωm) of the pure Bi_2S_3 at room temperature. Additionally, according to the electrical conductivity law of mixtures [20], the logarithm of the electrical conductivity can be expressed as follows:

$$\ln \sigma_T = V_M \ln \sigma_M + V_S \ln \sigma_S \quad (3)$$

where σ_T, V_M, σ_M, V_S, σ_S is the total electrical conductivity, volume fraction and electrical conductivity of matrix, volume fraction and electrical conductivity of the second phase, respectively. Because of the increased second $AgBi_3S_5$ phase with a high σ_S, the total electrical resistivity decreases again with increasing Ag content for the samples with $x \geq 0.02$, which are in agreement with the XRD (Fig. 2) and SEM (Figs. 3 and 4) analysis.

Fig. 5(b) shows the temperature dependence of the Seebeck coefficient (α) for $Bi_{2-x}Ag_{3x}S_3$. The negative α values indicate that all the samples are n-type semiconductors. The absolute value of the Seebeck coefficient ($|\alpha|$) decreases with increasing Ag content, which shows the same tendency with the electrical resistivity. The pure Bi_2S_3 sample shows the peak value of α about −480 μV/K at 323 K, while the α values for $Bi_{2-x}Ag_{3x}S_3$ ($x = 0.01$–0.06) samples range from −150 μV/K to −300 μV/K, which is lower than that of pure Bi_2S_3 sample. According to the expression $\alpha \approx \gamma - \ln n$ [21], where n and γ is the carrier concentration and scattering factor, respectively, the α is proportional to γ and inversely proportional to n. In the case of the pure Bi_2S_3, thermal activation could increase the carrier concentration, and plays a prominent role

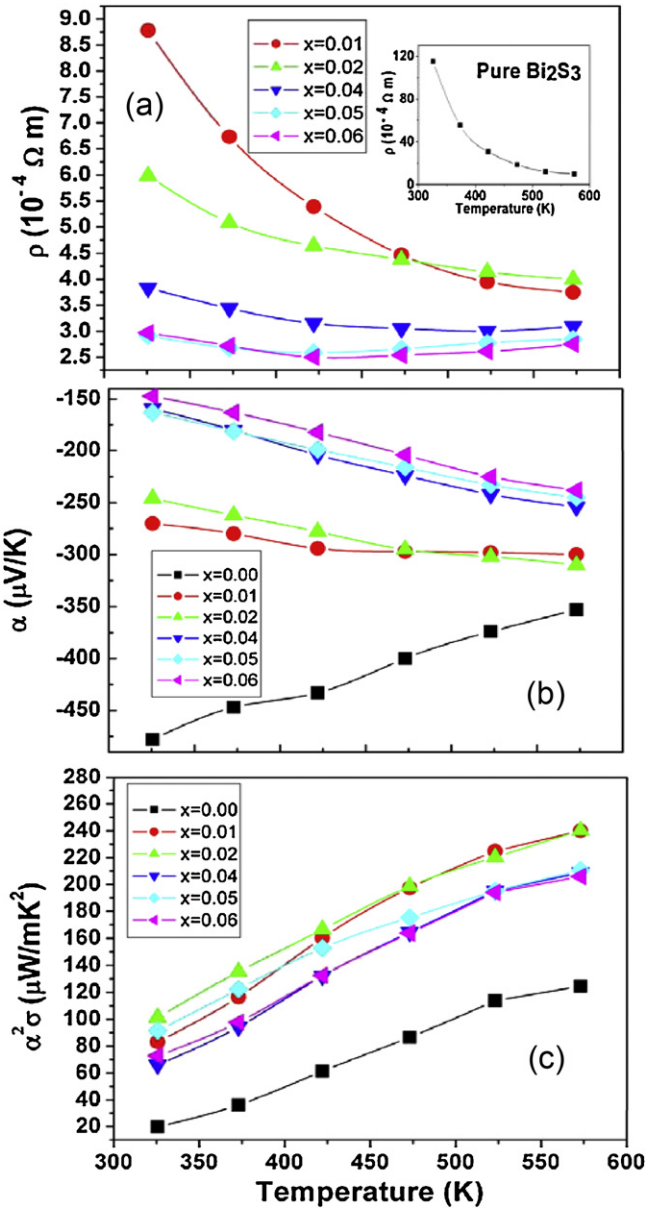

Fig. 5. Temperature dependence of electrical resistivity (a), Seebeck coefficient (b) and power factor (c) for $Bi_{2-x}Ag_{3x}S_3$ ($x = 0$, 0.01, 0.02, 0.04, 0.05, 0.06) bulk samples sintered by applying SPS at 673 K.

with increasing temperature, whereas the lattice thermal vibration which enlarges the scattering factor may make a dominate role for the Ag doped samples. All of these contribute to the results that the $|\alpha|$ value decreases with increasing temperature for the pure Bi_2S_3, but increases with increasing temperature for the Ag doped samples.

Fig. 5(c) shows the temperature dependence of the power factor (PF = $\alpha^2\sigma$) for $Bi_{2-x}Ag_{3x}S_3$. The Ag-doped samples show larger PF values than that of the undoped Bi_2S_3 sample. The maximum PF value is 241 μW/m/K^2 at 573 K for the $Bi_{1.98}Ag_{0.06}S_3$ ($x = 0.02$) sample, which is about two times higher than that of the pure Bi_2S_3 at the same temperature. The improved PF is attributed to the coupling effects of the electric conductivity and the Seebeck coefficient by optimizing Ag content.

Fig. 6 shows the temperature dependence of thermal conductivity (κ) for $Bi_{2-x}Ag_{3x}S_3$ ($x = 0$, 0.01, 0.02, 0.06). The thermal conductivity for all samples presents the same decreasing temperature dependent trend. The thermal conductivity of the Bi_2S_3 ranges

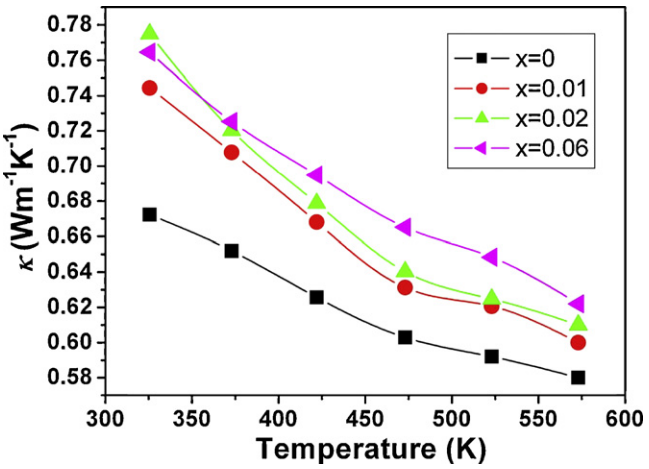

Fig. 6. Temperature dependence of thermal conductivity for $Bi_{2-x}Ag_{3x}S_3$ ($x = 0, 0.01, 0.02, 0.06$) bulk samples sintered by applying SPS at 673 K.

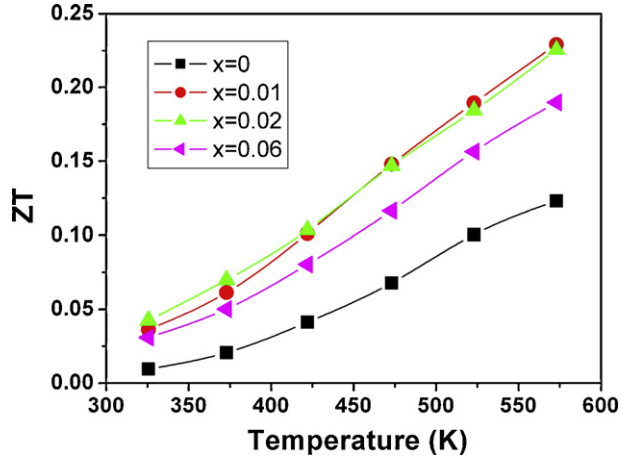

Fig. 7. Temperature dependence of the figure of merit (*ZT*) for $Bi_{2-x}Ag_{3x}S_3$ ($x = 0, 0.01, 0.02, 0.06$) bulk samples sintered by applying SPS at 673 K.

from 0.59 to 0.67 $W m^{-1} K^{-1}$ for the entire measured temperature range. Ag addition results in an increase of the thermal conductivity. The increased electronic thermal conductivity for the $Bi_{1.99}Ag_{0.03}S_3$ ($x = 0.01$) sample is caused by the increased carrier concentration [22], while the increased thermal conductivity of the $Bi_{2-x}Ag_{3x}S_3$ ($x = 0.02$ and 0.06) is due to the formation of the second $AgBi_3S_5$ phase with a high thermal conductivity (about 1.6 $W m^{-1} K^{-1}$ at the room temperature) [17]. The sample $Bi_{1.94}Ag_{0.18}S_3$ with the most second $AgBi_3S_5$ phases has the highest thermal conductivity.

Fig. 7 shows the temperature dependence of the dimensionless figure of merit (*ZT*) for the $Bi_{2-x}Ag_{3x}S_3$ ($x = 0, 0.01, 0.02, 0.06$) alloys. It is observed that the *ZT* value is enhanced by doping with Ag. The sample $Bi_{1.99}Ag_{0.03}S_3$ ($x = 0.01$) peaks the largest *ZT* value of 0.23 at 573 K, which is about twice that of Ag-free sample (0.11). The enhanced *ZT* value is mainly ascribed to the significantly increased electrical transport properties, which may be enhanced further by controlling the content and the distribution of the $AgBi_3S_5$ phase in the Bi_2S_3 matrix.

4. Conclusions

N-type $Bi_{2-x}Ag_{3x}S_3$ polycrystals were synthesized by a process combined mechanical alloying (MA) and spark plasma sintering (SPS) technique. With increasing Ag content, the electrical resistivity was reduced by tuning carrier concentration and the presence of the low-resistivity phase of $AgBi_3S_5$. The absolute value of the Seebeck coefficient shows an opposite temperature dependent trend compared with the resistivity. The power factor is enhanced from 122 $\mu W m^{-1} K^{-2}$ for pure Bi_2S_3 to 241 $\mu W m^{-1} K^{-2}$ for the $Bi_{1.98}Ag_{0.06}S_3$ sample, although the thermal conductivities of the samples increase with increasing Ag content, whereby a maximum *ZT* value of 0.23 was achieved at 573 K for the $Bi_{1.99}Ag_{0.03}S_3$ sample, which is about twice that of the pure Bi_2S_3 (0.11).

Acknowledgments

This work was supported byNational Natural Science Foundation of China (Grant No. 50972012), High-Tech 863 Program of China (Grant No. 2009AA03Z216), National Basic Research Program of China (Grant No. 2007CB607500), and Beijing Natural Science Foundation (Grant No. 2112028).

References

[1] B. Raton, CRC Handbook of Thermoelectrics, CRC, FL, USA, 1995.
[2] J.F. Li, W.S. Liu, L.D. Zhao, M. Zhou, High-performance nanostructured thermoelectric materials, NPG Asia Mater. 2 (2010) 152–158.
[3] G. Chen, M.S. Dresselhaus, G. Dresselhaus, J.P. Fleurial, T. Caillat, Recent developments in thermoelectric materials, Int. Mater. Rev. 48 (2003) 45–66.
[4] M. Prevel, O. Perez, J.G. Noudem, Bulk textured $Ca_{2.5}(RE)_{0.5}Co_4O_9$ (RE: Pr, Nd, Eu Dy and Yb) thermoelectric oxides by sinter-forging, Solid State Sci. 9 (2007) 231–235.
[5] M. Stordeur, D.M. Row, Handbook of Thermoelectrics, CRC Press, Boca Raton, 1995, 239 p.
[6] L.D. Zhao, B.P. Zhang, J.F. Li, M. Zhou, W.S. Liu, Effects of process parameters on electrical properties of n-type Bi_2Te_3 prepared by mechanical alloying and spark plasma sintering, Physica B 400 (2007) 11–15.
[7] X.F. Tang, W.J. Xie, H. Li, W.Y. Zhao, Q.J. Zhang, M. Niino, Preparation and thermoelectric transport properties of high-performance p-type Bi_2Te_3 with layered nanostructure, Appl. Phys. Lett. 90 (2007) 012102–12111.
[8] M. Zhou, J.F. Li, T. Kita, Nanostructured $AgPb_mSbTe_{m+2}$ system bulk materials with enhanced thermoelectric performance, J. Am. Chem. Soc. 130 (2008) 4527–4532.
[9] A. Cantarero, J. Martinez-Pastor, A. Segura, Transport properties of bismuth sulfide single crystals, Phys. Rev. B 35 (1987) 9586–9590.
[10] B. Chen, C. Uher, L. Iordanidis, M.G. Kanatzidis, Chem. Mater. 9 (1997) 1655–1658.
[11] H.T. Shaban, M.M. Nassary, M.S. El-Sadek, Physica B 403 (2008) 1655–1659.
[12] L.D. Zhao, B.P. Zhang, W.S. Liu, H.L. Zhang, J.F.J. Li, Enhanced thermoelectric properties of bismuth sulfide polycrystals prepared by mechanical alloying and spark plasma sintering, J. Solid State Chem. 181 (2008) 3278–3282.
[13] T. Kyratsi, D.Y. Chung, M.G. Kanatzidis, Bi/Sb distribution and its consequences in solid solution members of the thermoelectric materials $K_2Bi_{8-x}Sb_xSe_{13}$, J. Alloys Compd. 338 (2002) 36–42.
[14] J.L. Cui, W.J. Xiu, L.D. Mao, P.Z. Ying, L. Jiang, X. Qian, Transport properties of quaternary Ag–Bi–Sb–Te alloys prepared by pressureless sintering, J. Solid State Chem. 180 (2007) 1158–1162.
[15] D.P. White, P.G. Klemens, Thermal conductivity of thermoelectric $Si_{0.8}$–$Ge_{0.2}$ alloys, J. Appl. Phys. 71 (1992) 4258–4263.
[16] M. Omori, Sintering, consolidation, reaction and crystal growth by the spark plasma system (SPS), Mater. Sci. Eng. A 287 (2000) 183–188.
[17] J.H. Kim, D.Y. Chung, D. Bilc, S. Loo, J. Short, S.D. Mahanti, T. Hogan, M.G. Kanatzidis, Chem. Mater. 17 (2005) 3606–3614.
[18] Z.H. Ge, B.P. Zhang, P.P. Shang, Y.Q. Yu, C. Chen, J.F. Li, J. Electron. Mater. 40 (2011) 1087–1094.
[19] Z.H. Ge, B.P. Zhang, Z.X. Yu, J.F. Li, J. Mater. Res. 26 (2011) 2711–2718.
[20] Z.D. Guan, Z.T. Zhang, J.S. Jiao, Physical Properties of Inorganic Materials, Tsinghua University Press, Beijing, China, 2002, 265 p.
[21] X.D. Liu, Y.H. Park, Mater. Trans. 43 (2002) 681–687.
[22] S. Ohta, T. Nomura, H. Ohta, M. Hirano, H. Hosono, K. Koumoto, Appl. Phys. Lett. 87 (2005) 092108.